

RESEARCH

Open Access



Experimental Investigation on the Mechanical Properties of Polypropylene Hybrid Fiber-Reinforced Roller-Compacted Concrete Pavements

Ninghui Liang^{1*} , Xiufei You¹, Ru Yan², Qingxu Miao³ and Xinrong Liu¹

Abstract

To explore the effect of multi-scale polypropylene fiber (PPF) hybridization on the mechanical properties of roller-compacted concrete (RCC), the early-age (3, 7, 14, 28 days) compressive strength, splitting tensile strength and uniaxial tensile test of RCC reinforced with micro-, macro- and hybrid polypropylene fibers were investigated. Then, the tensile stress–strain curve of polypropylene fiber-reinforced roller-compacted concrete (PFRCC) and the corresponding tensile parameters were obtained. The uniaxial tensile constitutive equation of PFRCC and fiber hybrid effect function was also proposed. Finally, the enhancement mechanism of fiber hybridization on mechanical properties of RCC was analyzed. The results indicated that the strength and toughness of PFRCC improved with the incorporation of PPF, showing obvious plastic failure characteristics of PFRCC. Before curing the concrete for 7 days, micro-PPF played a major role in strengthening RCC, while macro-PPF played a major role in reinforcing concrete after that. Moreover, the tensile strength and toughness indexes of multi-scale PFRCC performed the best, indicating the positive hybridization of three types of PPF. The proposed PFRCC uniaxial tensile constitutive equation and fiber hybrid effect function based on existing researches were also well matched with the experimental results.

Keywords: roller-compacted concrete, multi-scale polypropylene fibers, stress–strain curve, mechanical properties, hybrid effect function

1 Introduction

Roller-compacted concrete (RCC) is commonly used in a variety of road pavements, pavement bases and et al. (Lopez-Uceda et al., 2016), which is known for saving cement, early high strength and reducing construction time. However, RCC also includes some disadvantages, such as low tensile strength, poor crack resistance and toughness, limiting its development in engineering structures (Bayagoob & Bamaga, 2019; Lam et al., 2018). Previous studies (Ahmad & Umar, 2018; Benouadah et al.,

2017; Marushchak et al., 2019; Yoo & Banthia, 2016) have shown that the addition of fibers can effectively control the formation and development of cracks in concrete, and greatly increase the strength and toughness of concrete.

In practical engineering applications, there are many kinds of fibers, among which steel fiber and polypropylene fiber (PPF) are the most popular (Hussain et al., 2020; Madhkhan et al., 2012). Steel fiber has high elastic modulus and stiffness, which is widely used for its good strengthening and toughening effect on concrete. However, its development is limited by its deficiencies of high cost, poor corrosion resistance and inconvenient construction. PPF is often divided into micro-PPF and macro-PPF according to the size. Micro-PPF can restrain

*Correspondence: liangninghui0705@163.com

¹ School of Civil Engineering, Chongqing University, Chongqing, China
Full list of author information is available at the end of the article
Journal information: ISSN 1976-0485 / eISSN 2234-1315

the early cracks of concrete significantly, but it has no obvious reinforcing and toughening effect on concrete. Macro-PPF, also known as the candidate material of steel fiber, has comparable reinforcing and toughening effect with steel fiber (Yin et al., 2015). Many researches showed that the hybrid fiber-reinforced concrete can make different fibers complement each other and promote the mechanical properties of the concrete matrix (Turk et al., 2021; Yao et al., 2003). Especially, the hybrid addition of micro- and macro-PPFs in a certain proportion in the concrete matrix performed better than the addition of a single fiber (Hsie et al., 2008; Liang et al., 2016).

The properties of RCC reinforced with PPFs have been concerned by many scholars in recent decades (Aghaeipour & Madhkhan, 2019). Yazici et al. (2015) researched the effects of micro-PPF on mechanical properties of RCC and showed that the mechanical properties of RCC reduced by 20% with the addition of PPF, while the fracture impacts and toughness increased. However, Madhkhan et al. (2011) indicated that the addition of micro-PPF increased the compressive strength of RCC mixtures by 10.3%. Some researches (LaHucik et al., 2017; Rooholamini et al., 2018) also showed that the addition of macro-PPF can promote the residual strength and toughness of RCC significantly. Additionally, the research on concrete uniaxial tensile constitutive model had also attracted the attention of scholars (Deng et al., 2020; Ding & Yan, 2011; Pyo et al., 2017). It is not only the main basis for studying the strength theory and fracture mechanism of concrete, but also an important factor affecting the cracking and durability of concrete structures. Based on the experimental analysis of axial tensile stress–strain curve of concrete reinforced with steel fiber and PPF, Xu et al. (2014) put forward the axial tensile stress–strain relationship curve equation of steel–polypropylene hybrid fiber-reinforced concrete with respect to fiber content and length-to-diameter ratio. At present, the stress–strain curves and mechanical properties of concrete reinforced with different types of fibers have been researched by many researchers, but the report about the influence of hybrid fibers of different sizes on mechanical properties and constitutive model of RCC are rare. Yuan et al. (2020) investigated the synergy effect in the performance of no-slump high-strength high-ductility (NSHSDC) based on polyethylene and steel fibers,

and showed that the hybridization of fibers of different lengths significantly improved the strength, toughness, and energy absorbing capacity. Liang et al. (2021) also carried out uniaxial compressive test on RCC mixed with PPFs of three types to investigate the effects of hybrid fibers on the uniaxial compressive stress–strain curve of RCC, and found that the hybridization of PPFs improved the compressive strength and toughness.

To further study the effect of hybrid PPFs on the mechanical behavior of RCC, 8 groups of polypropylene fiber-reinforced roller-compacted concrete (PFRCC) specimens were designed in this paper. The compressive and splitting tensile strength of RCC reinforced with macro-, micro- and hybrid polypropylene fibers in early-stage (3, 7, 14, 28 days) were investigated, as well as the uniaxial tensile stress–strain curve. According to the experimental results, the strengthening effect of hybrid PPFs on the performance of PFRCC and the characteristics of the uniaxial tensile stress–strain full curve were explored. The nonlinear fitting analysis of the uniaxial tensile stress–strain curve of PFRCC was carried out based on the existing tensile constitutive model, and the effect of fiber hybridization on the constitutive mechanical indexes was also discussed, providing reference for future research and practical engineering.

2 Material and Methods

2.1 Materials and Mix Proportions

Cementing material: Portland cement P-O 52.5R, and the physical and chemical properties of the cement were investigated according to the guidance of Chinese standard GB/T1346-2011 and GB/T 17671-1999, as presented in Table 1; Coarse aggregates: crushed gravel of diameter 5–10 mm and 10–20 mm, with continuous gradation. The apparent densities and bulk densities of 5–10 mm coarse aggregate were 2670 and 1440 kg/m³, and those of 10–20 mm coarse aggregate were 1460 and 2700 kg/m³, respectively; fine aggregates: sands with fineness moduli of 2.89, which was well graded according to Chinese standard JGJ52-2006, as shown in Fig. 1; water reducer: polycarboxylic superplasticizer with the water reducing rate of 28%, meeting the requirements of Chinese Standard GB8076-2008; Fibers: two types of fasciculate monofilament micro-PPFs and one type of corrugated macro-PPF. The physical and mechanical properties and

Table 1 The physical and chemical properties of the cement.

| Specific surface area /(m ² /kg) | Soundness/mm | Setting time /min | | Flexural strength /MPa | | Compressive strength /MPa | |
|---|--------------|----------------------|--------------------|------------------------|-----|---------------------------|------|
| | | Initial setting time | Final setting time | 3d | 28d | 3d | 28d |
| 350 | 1.0 | 190 | 242 | 6.6 | 9.1 | 29.0 | 57.6 |

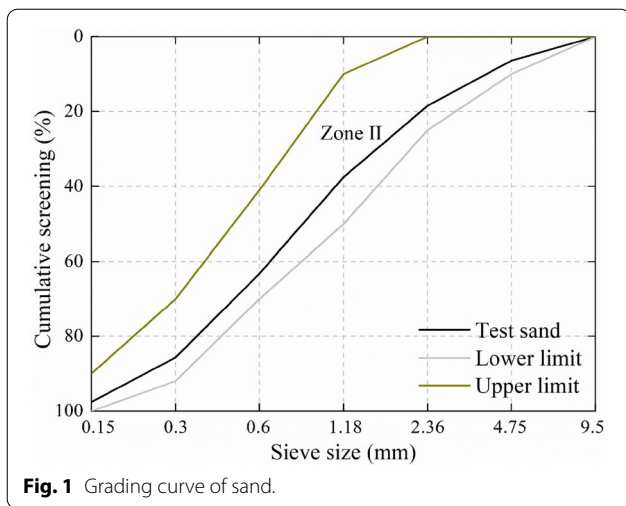


Fig. 1 Grading curve of sand.

appearance of micro-PPFs (FF1 and FF2) and macro-PPF (CF) are shown in Table 2 and Fig. 2, respectively.

According to previous experiments (Liang et al., 2021; Liu et al., 2015) and engineering experience, the optimal dropping contents of micro-PPF and macro-PPF were 0.9 and 6 kg/m³, respectively. The mix proportion design of C50 strength grade RCC pavements was conducted according to Chinese standard JGJ55-2011 and DL/T5330-2015. Considering the influence of fiber incorporation on the workability of RCC and the slump of RCC less than 10, the mixture ratio of concrete matrix was obtained after some repeated adjustments. Nine groups

of RCC specimens, A0~A8, were designed according to the fiber type and hybridization. Specimens A0 were RCC without fiber, which was the reference for other groups. Specimens A1 and A2 were mixed with only micro-PPFs, while specimens A3 only incorporated macro-PPFs. Specimens A4, A5 and A6 were mixed with two fiber types, and specimens A7 and A8 were mixed with three different types of PPFs. The mixture ratio of each concrete matrix remained consistent, which guaranteed the comparability of experimental results, as shown in Table 3.

2.2 Specimen Preparation

In order to ensure the uniform distribution of fibers in the concrete matrix, the coarse and fine aggregates were firstly poured into the mixer. PPF was evenly and dispersedly sprinkled into the mixer after 1 min of mixing, and continued to be stirred for about 2 min. No obvious balling was observed during the mixing. Then cements were poured and stirred for mixing 2 min. Finally, the water and water reducer were slowly poured into mixtures, and mixtures were poured out and molded after stirring for about 2 min. In order to reduce the voids in casting RCC specimens, a heavy steel plate smaller than the size of the specimen mold was prepared for compaction according to Chinese standard GB/T50081-2019. The Vebe consistency of mixtures was measured in reference to Chinese standard GB/T 50080-2016 and the results are shown in Table 4. After 24 h, the fresh concrete was removed from

Table 2 The physical and mechanical properties of polypropylene fibers.

| Fiber type | Diameter/mm | Length/mm | Aspect ratio | Tensile strength/MPa | E/GPa | Elongation/% | Density/g·cm ⁻³ | Alkali resistance/% | Recommended content/kg m ⁻³ |
|------------|-------------|-----------|--------------|----------------------|-------|--------------|----------------------------|---------------------|--|
| FF1 | 0.026 | 19 | 730.77 | 641 | 4.5 | 40 | 0.91 | 99.8 | 0.9 |
| FF2 | 0.1 | 19 | 190 | 472 | 5.8 | 19.9 | 0.91 | 99.8 | 0.9 |
| CF | 0.8 | 50 | 62.5 | 706 | 7.4 | 10.0 | 0.95 | 99.7 | 6.0 |

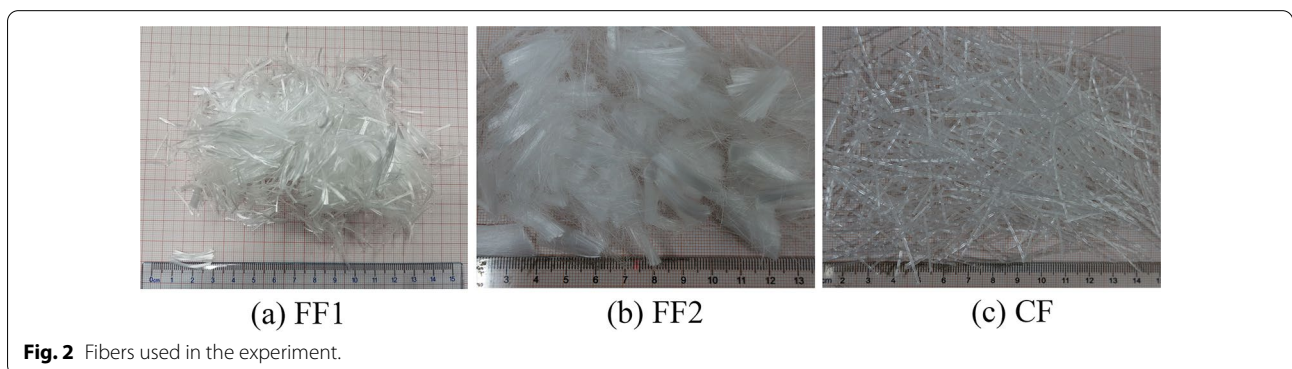


Fig. 2 Fibers used in the experiment.

Table 3 Mixture ratio of C50 RCC/(kg/m³).

| Specimen no. | Fiber type | Cement | Sand | Coarse aggregate | | Water | Fiber content | Water reducer /% |
|--------------|------------|--------|------|------------------|----------|-------|---------------|------------------|
| | | | | 5~10 mm | 10~20 mm | | | |
| A0 | NO | 456 | 787 | 505 | 505 | 164 | 0 | 1 |
| A1 | FF1 | 456 | 787 | 505 | 505 | 164 | 0.9 | 1 |
| A2 | FF2 | 456 | 787 | 505 | 505 | 164 | 0.9 | 1 |
| A3 | CF | 456 | 787 | 505 | 505 | 164 | 6.0 | 1 |
| A4 | FF1+CF | 456 | 787 | 505 | 505 | 164 | 0.6+5.4 | 1 |
| A5 | FF1+CF | 456 | 787 | 505 | 505 | 164 | 0.9+5.1 | 1 |
| A6 | FF1+CF | 456 | 787 | 505 | 505 | 164 | 1.2+4.8 | 1 |
| A7 | FF1+FF2+CF | 456 | 787 | 505 | 505 | 164 | 0.45+0.45+5.1 | 1 |
| A8 | FF1+FF2+CF | 456 | 787 | 505 | 505 | 164 | 0.6+0.6+4.8 | 1 |

Table 4 Vebe consistency of RCC mixtures.

| Specimen no. | A0 | A1 | A2 | A3 | A4 | A5 | A6 | A7 | A8 |
|-------------------------|----|----|----|----|----|----|----|----|----|
| Vebe consistency time/s | 23 | 24 | 26 | 28 | 27 | 27 | 25 | 27 | 25 |

the mold and moved into the standard curing room for curing.

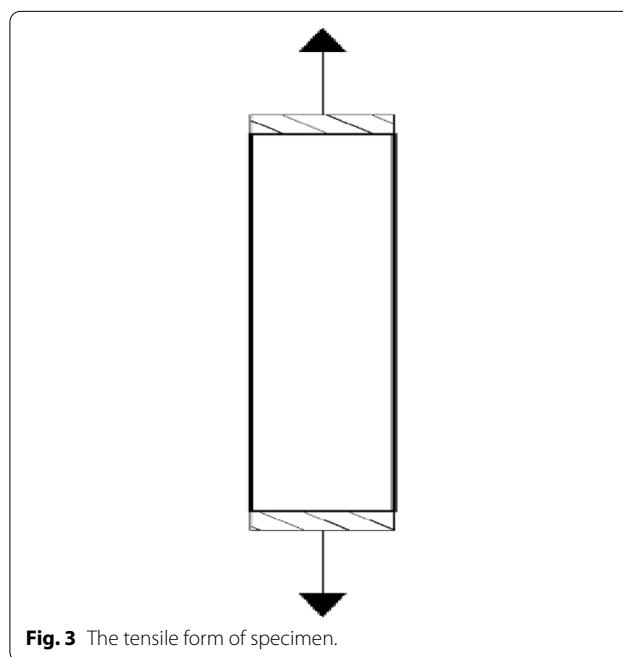
2.3 Mechanical Tests

In accordance with the Chinese standard GB/T50081-2019, the compressive and splitting tensile strength of RCCs at different curing ages (3 d, 7 d, 14 d, 28 d) were carried out using 100 mm cubic specimens and values were averaged for 3 specimens for each RCC series, with 216 cubic specimens in total. The uniaxial tensile tests were performed using 100 mm × 100 mm × 300 mm prismatic specimens in accordance with Chinese standard CECS 13:2009. The testing results were averaged from six specimens for each series, due to the difficulties such as uncertain fracture position and easy eccentricity in testing process (Cattaneo et al., 2009; Olivito & Zucarello, 2010). The uniaxial tensile test was carried out by sticking steel plate at the end of prismatic specimen with equal section, as shown in Fig. 3. The displacement controlled uniaxial tensile tests were performed with an INSTRON-1342 electronic hydraulic servo testing machine at a loading rate of 0.1 mm/min. Two liner variable differential transducers were used to measure the elongation with the gauge length of 80 mm, as presented in Fig. 4.

3 Results and Discussion

3.1 Compressive Strength

The compressive failure of plain RCC A0 specimens presented obvious brittle failure. The failure modes of A1 and A2 specimens added with micro-PPFs

**Fig. 3** The tensile form of specimen.

were similar to those of A0 specimens, but their failure shapes were relatively complete due to the bonding effect of fibers. The addition of macro-PPFs maintained the integrity of PFRCC A3~A8 specimens and improved the compressive toughness of RCC. The compressive strength results of each group of specimens at different curing ages are presented in Fig. 5. The compressive strength of RCC increased or



Fig. 4 Device of uniaxial tensile test.

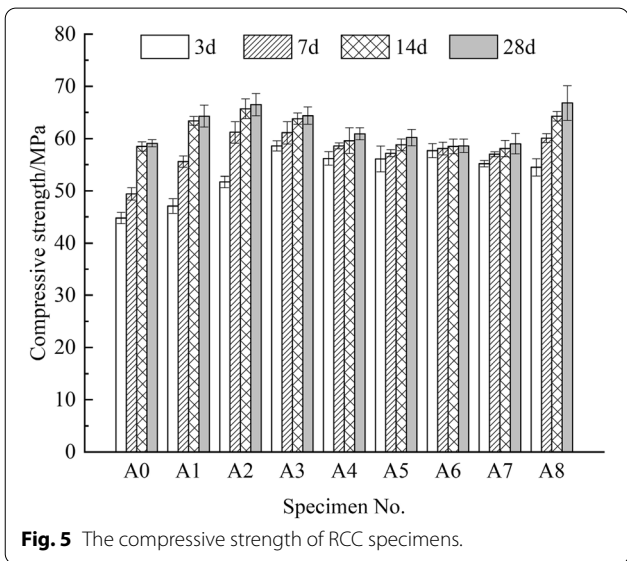


Fig. 5 The compressive strength of RCC specimens.

slightly decreased with the hybridization of different PPFs. Moreover, the early-age compressive strength of all groups was at a high level, which was in line with the characteristics of fast hardening and early strength of RCC. At the early age, the incorporation of PPFs improved the compressive strength of RCC obviously, and macro-PPFs showed better reinforcement effect in RCC matrix with the increasing of curing ages. Compared with plain RCC at 28 curing ages, adding micro-fibers FF1 and FF2 at 0.9 kg/m^3 can increase 8.8% and 12.52%, respectively. FF2 showed a better effect than FF1 in improving the compressive strength of RCC, due to the higher diameter resulting in an increase of the interfacial area and interface bond strength between the matrix and the fiber (Simões et al., 2017). Adding macro-fibers CF at 6 kg/m^3 , the strength improved by

8.97%. The compressive strength of multi-scale PFRCC A8 group (dropped with three kinds of PP fibers) improved the most at 13.03%. The A8 group all showed superior compressive strength at different curing ages.

3.2 Splitting Tensile Strength

In the splitting tensile test, the plain RCC A0 failed rapidly from cracking to fracture, showing obvious brittleness characteristics. The shorter the curing ages, the faster the failure process. With the increase of curing ages, the cracking growth of A1 and A2 specimens added with micro-PPFs slowed down and gradually closed to ductile failure. However, the failure of A3~A8 specimens mixed with macro-PPFs showed obvious toughness characteristics. The macro-PPFs in concrete had obvious effect on inhibiting crack propagation and bridging the concrete matrix, maintaining the integrity of concrete matrix and making concrete matrix still have a certain bearing capacity after failure. Fig. 6 shows the splitting tensile strength of specimens at different curing ages. The splitting tensile strength of all groups improved with the increase of curing ages. Relative to the RCC control mixture A0 after curing for 3 days, the splitting tensile strength of A2 incorporated with micro-PPFs was 4.74 MPa increasing by 32.03%, indicating that the incorporation of PPFs in RCC played a strengthening role at the early stage of curing. As the increasing of curing days, the splitting tensile strength of RCC mixed with hybrid PP fibers improved more. After curing for 28 days, the multi-scale PFRCC A7 reached the highest splitting tensile strength of 5.49 MPa. Therefore, the mixing of PPFs of different sizes is more conducive to the development of the splitting tensile strength of RCC at different

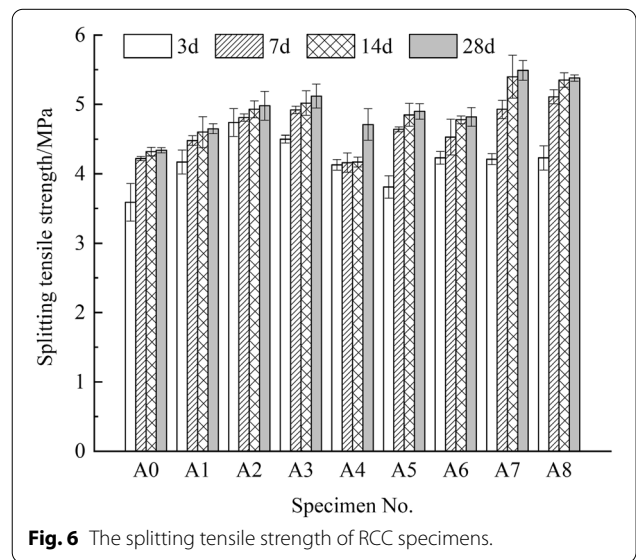


Fig. 6 The splitting tensile strength of RCC specimens.

curing ages, showing a significant positive hybrid effect. The reinforcing effect of macro-PPF is better than that of micro-PPF.

3.3 Uniaxial Tensile Performance

3.3.1 Failure Process

The typical failure modes of RCC specimens are presented in Fig. 7. The specimens A0 without fiber and A1 ~ A2 reinforced with micro-PPF failed suddenly and broke in the weakest section, as exhibited in Fig. 7(a). The failure rarely occurred at the bonding place between the steel plate and the specimen. The addition of macro-PPF had an obvious effect on improving the failure mode of specimens. The failure of A3 ~ A8 specimens mixed with macro-PPF started with microcracking, and showed the characteristics of obvious toughness due to the significantly bridging effect of macro-PPF, as shown in Fig. 7(b). The inclination of failure plane was random, and all specimens had a failure plane approximately perpendicular to the load applied. Compared with RCC, the tensile failure surface of PFRCC was more uneven due to the pulling out or breaking of PPFs. The load–displacement curves of RCC specimens under the uniaxial tensile load are shown in Fig. 8. Before the tensile load reached the peak value in Fig. 8, A3 ~ A8 specimens mixed with macro-PPF also behaved similarly as A0 ~ A2 specimens. With the increase of tensile displacement, the microcracks in the RCC matrix gradually expanded and connected, and the macro-PPF gradually played a bridging role at the cracks. When the fibers on both sides of the microcrack were no longer able to withstand the maximum stress, the fibers deformed or pulled out from the RCC matrix. Then, the macrocrack gradually appeared on the surface of the specimen mixed with macro-PPF. The bearing capacity of PFRCC decreased relatively slowly or remained within

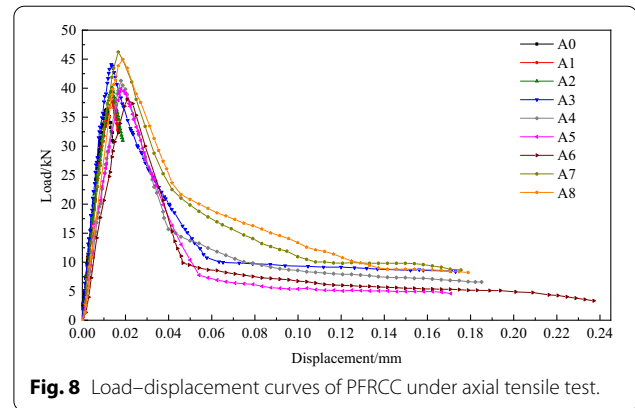


Fig. 8 Load–displacement curves of PFRCC under axial tensile test.

a certain range. Finally, the loading stopped due to the excessive deformation of specimens and the specimen failed (Hu et al., 2018).

3.3.2 Load–Displacement Curve

As shown in Fig. 8, the specimens underwent a failure process from elastic deformation to plastic deformation. In the linear elastic stage, the incorporation of PPF had no obvious effect on the tensile performance of RCC. With the incorporation of PPF of different types and mixing proportion, the descending section of the load–displacement curve performed differently for each group of specimens. The curve descending section of A0 ~ A2 specimens mixed with micro-PPF was steep and incomplete, while the strain hardening phenomenon of specimen A3 reinforced with macro-PPF and A4 ~ A6 specimens reinforced with hybrid PP fibers was obvious. The slope of the descending section after the peak of the multi-scale PFRCC specimens A7 and A8 was smaller than that of the other groups, and it was obvious that the area under the curve of these two groups of curves was larger than that of the other groups.



(a) The failure location of specimens



(b) The failure surface of PFRCC

Fig. 7 Failure patterns of RCC specimens in uniaxial tensile test.

When there is an obvious inflection point in the descending section of A3~A6 curve of the specimens mixed with macro-PPF, there were even two inflection points in the descending section of A7~A8 curve of multi-scale PFRCC. After the first inflection point, the tensile stress–strain curve tended to flatten with the increase of strain. The main fracture surface of PFRCC had been formed. At this stage, the tensile stress of the macro-PPFs at the fracture surface increased continuously, leading to the deformation of the macro-PPFs in concrete matrix. The macro-PPFs in the anchorage zone on both sides of the fracture surface will pull out and slip in varying degrees. After the second inflection point, the strain increased rapidly, the stress decreased slowly and the curve became smooth. At this time, the fracture failure surface continued to develop and widen, the micro-PPFs failed at the section, the macro-PPFs were gradually pulled out or broken, and the load on the specimen were mainly borne by the macro-PPFs (Xu et al., 2014). However, due to the randomness of the fiber location in concrete matrix and the inevitable test error, the appearance of the two inflection points may not be certain in all specimens mixed with micro- and macro-PPFs.

3.3.3 Strength and Toughness

According to the uniaxial load–displacement curves of specimens and Chinese Standard CECS 13:2009, the uniaxial tensile strength f_t , the corresponding peak tensile strain ε_t , the uniaxial tensile energy $W_{0.2}$, and the uniaxial tensile toughness ratio $R_{e,0.2}$ were calculated by Eqs. (1, 2, 3, 4), as shown in Table 5:

$$f_t = \frac{F_{at,max}}{A}, \quad (1)$$

$$\varepsilon_t = \frac{u_{at,max}}{L_0}, \quad (2)$$

Table 5 Uniaxial tensile strength and toughness of PFRCC.

| Specimen no. | f_t /MPa | ε_t / $\mu\varepsilon$ | $W_{0.2}$ /N·m | $R_{e,0.2}$ |
|--------------|------------|------------------------------------|----------------|-------------|
| A0 | 3.62 | 151.62 | 0.76 | 0.059 |
| A1 | 3.75 | 176.28 | 0.92 | 0.068 |
| A2 | 3.98 | 170.06 | 1.12 | 0.078 |
| A3 | 4.39 | 181.43 | 5.28 | 0.334 |
| A4 | 4.13 | 229.17 | 4.90 | 0.330 |
| A5 | 4.02 | 253.04 | 4.02 | 0.278 |
| A6 | 3.90 | 276.91 | 4.17 | 0.297 |
| A7 | 4.64 | 224.93 | 6.32 | 0.378 |
| A8 | 4.53 | 239.43 | 6.59 | 0.404 |

All data in the table are mean values.

$$W_{0.2} = \int_0^{0.002L_0} F_{at}(u_{at}) du_{at}, \quad (3)$$

$$R_{e,0.2} = \frac{W_{0.2}}{f_t \times A \times L_0 \times 0.2\%}, \quad (4)$$

where $u_{at,max}$ is the peak displacement; $F_{at}(u_{at})$ represents the load–displacement curve function of uniaxial tension; u_{at} is the uniaxial tensile displacement; L_0 represents the standard distance of tensile deformation measurement; A represents the section area of the specimen.

It can be observed from Table 5 that the incorporation of PPF improved f_t and ε_t of RCC. For the RCC mixed with only one fiber type, the f_t and ε_t of macro-PPF mixed with RCC were higher than those of RCC reinforced with micro-PPF, showing the macro-PPF was better than the micro-PPF in strengthening and toughening of RCC. However, compared with A3 blended with macro-PPF, the f_t and ε_t of multi-scale PFRCC specimens A7 and A8 increased by 3~6% and 24~32%, respectively, showing positive hybrid effect of PPFs of three types. Additionally, the incorporation of PPF also promoted the $W_{0.2}$ and $R_{e,0.2}$ of specimen of each group, which was attributed to the fact that the fibers at the cracks gradually played a bridging role with the expansion of cracks. Relative to plain RCC A0, the $R_{e,0.2}$ of specimens mixed with only micro-PPF and specimens incorporated with macro-PPF increased by 15~32% and 466%, respectively. The $W_{0.2}$ and $R_{e,0.2}$ of multi-scale PFRCC specimens A8 were the highest of all testing series, which were 767% and 585% higher than that of control group A0. The improvement of tensile parameters may be attributed to the uniform distribution of multi-scale PPFs in RCC, and PPFs of different type played a part in different cracking stages of RCC to improve the strength and toughness.

3.3.4 Constitutive Models

The gentle descending section of the uniaxial tensile stress–strain curve of RCC reflects the effect of fiber incorporation, and the strain hardening phenomenon will occur when the bearing capacity drops to a certain value. The descending section of some uniaxial tensile stress–strain curve models proposed in previous studies is too steep and cannot be adapted to fiber-reinforced concrete well (Guo and Shi, 2003). The uniaxial tensile constitutive equation of concrete proposed in Chinese standard GB 50010-2010 may be suitable for fitting the uniaxial tensile stress–strain curve of PFRCC. The descending section of the uniaxial stress–strain curve in the model is mainly dominated by shape factor α_t (the smaller α_t is, the gentler the descending section is). The adjustment of parameters greatly promotes the applicability of the model to

Table 6 Measured values of elastic modulus of PFRCC in each group.

| Specimen no. | A0 | A1 | A2 | A3 | A4 | A5 | A6 | A7 | A8 |
|--------------|------|------|------|------|------|------|------|------|------|
| E_c /GPa | 43.7 | 44.5 | 45.6 | 45.0 | 43.6 | 45.1 | 43.1 | 44.5 | 42.1 |

fiber-reinforced concrete. The relevant formulas are as below:

$$\sigma_t = \begin{cases} \rho_t(1.2 - 0.2x^5)E_c\varepsilon_t x & (\varepsilon \leq \varepsilon_t) \\ \frac{\rho_t x}{\alpha_t(x - 1)^{1.7} + x} E_c \varepsilon_t & (\varepsilon > \varepsilon_t) \end{cases}, \quad (5)$$

$$\rho_t = \frac{f_t}{E_c \varepsilon_t}, \quad (6)$$

$$x = \frac{\varepsilon}{\varepsilon_t}, \quad (7)$$

where E_c is the compressive elastic modulus of RCC, which is measured by the test, as shown in Table 6.

The average uniaxial tensile stress–strain curves of each group of specimens were nonlinearly fitted to obtain the shape factor α_t and correction determination coefficient R^2 of the descending section of the curve, as shown in Table 7. The fitting results are shown in Fig. 9. It can be seen from the fitting results that the correction determination coefficient R^2 are greater than 0.97 for all testing groups, and the fitting curve is in good agreement with the test data, indicating that the concrete uniaxial tensile constitutive model provided by the Chinese standard GB 50010-2010 is suitable for PFRCC.

As shown in Eqs. (5, 6, 7), the uniaxial tensile constitutive model of PFRCC was controlled by four mechanical indexes: the uniaxial tensile strength f_t , the corresponding peak tensile strain ε_t , the elastic modulus E_c , and the shape factor of descending stage α_t . In order to explore the PPF hybrid effect on the four mechanical indexes of uniaxial tensile constitutive model of PFRCC, the fiber hybrid effect function was proposed based on the method of second-order model applied in response surface methodology (RSM) (Liang et al., 2021), as given in Eq. (8)~(9). λ is the characteristic value of fiber and is an independent variable of fiber hybrid effect

function, reflecting the fiber volume fraction and size characteristics:

$$\lambda = V_f \frac{l_f}{d_f}, \quad (8)$$

$$W = 1 + P_1 \lambda_i + P_2 \lambda_j + P_3 \lambda_k + P_4 \lambda_i^2 + P_5 \lambda_j^2 + P_6 \lambda_k^2 + P_7 \lambda_i \lambda_j + P_8 \lambda_k \lambda_j + P_9 \lambda_i \lambda_k + P_{10} \lambda_i \lambda_j \lambda_k, \quad (9)$$

where V_f is the volume fraction of PPF, as given in Table 8. l_f is the length of PPF, d_f is the equivalent diameter of PPF, $P_1 \sim P_{10}$ are the undetermined parameter, W is the increase factor (ratio of a certain mechanical index of PFRCC and plain RCC), $\lambda_i, \lambda_j, \lambda_k$ are the characteristic values of FF1, FF2 and CF, respectively. The fiber characteristic values are also listed in Table 8 according to Eq. (8).

Some researchers indicated that the relationship between fiber characteristic value λ and the strength or toughness of concrete is a quadratic function (Lisantonio et al. 2017; Shao, 2011). Considering that the content of single fiber is the quadratic function peak value, Eq. (9) can be simplified as Eq. (10):

$$W = 1 - 2 \times 0.72 P_4 \lambda_i - 2 \times 0.188 P_5 \lambda_j - 2 \times 0.395 P_6 \lambda_k + P_4 \lambda_i^2 + P_5 \lambda_j^2 + P_6 \lambda_k^2 + P_7 \lambda_i \lambda_j + P_8 \lambda_k \lambda_j + P_9 \lambda_i \lambda_k + P_{10} \lambda_i \lambda_j \lambda_k. \quad (10)$$

According to Eq. (10) and the statistical analysis of the four mechanical indexes in Tables 5, 6 and 7, the undetermined parameters $P_4 \sim P_{10}$ were fitted and the fiber hybrid effect function is presented in Table 9. The predicted values of the four mechanical indexes were in good agreement with the fitting values based the testing results, which were reflected by correction determination coefficient R^2 , also as shown in Table 9.

Table 7 The fitted value α_t and correction decision coefficient of RCC in each group.

| Specimen no. | A0 | A1 | A2 | A3 | A4 | A5 | A6 | A7 | A8 |
|--------------|-------|-------|-------|-------|-------|-------|-------|-------|-------|
| α_t | 2.34 | 2.33 | 1.85 | 1.13 | 1.69 | 2.36 | 2.57 | 1.21 | 1.11 |
| R^2 | 0.998 | 0.996 | 0.996 | 0.997 | 0.997 | 0.997 | 0.975 | 0.998 | 0.998 |

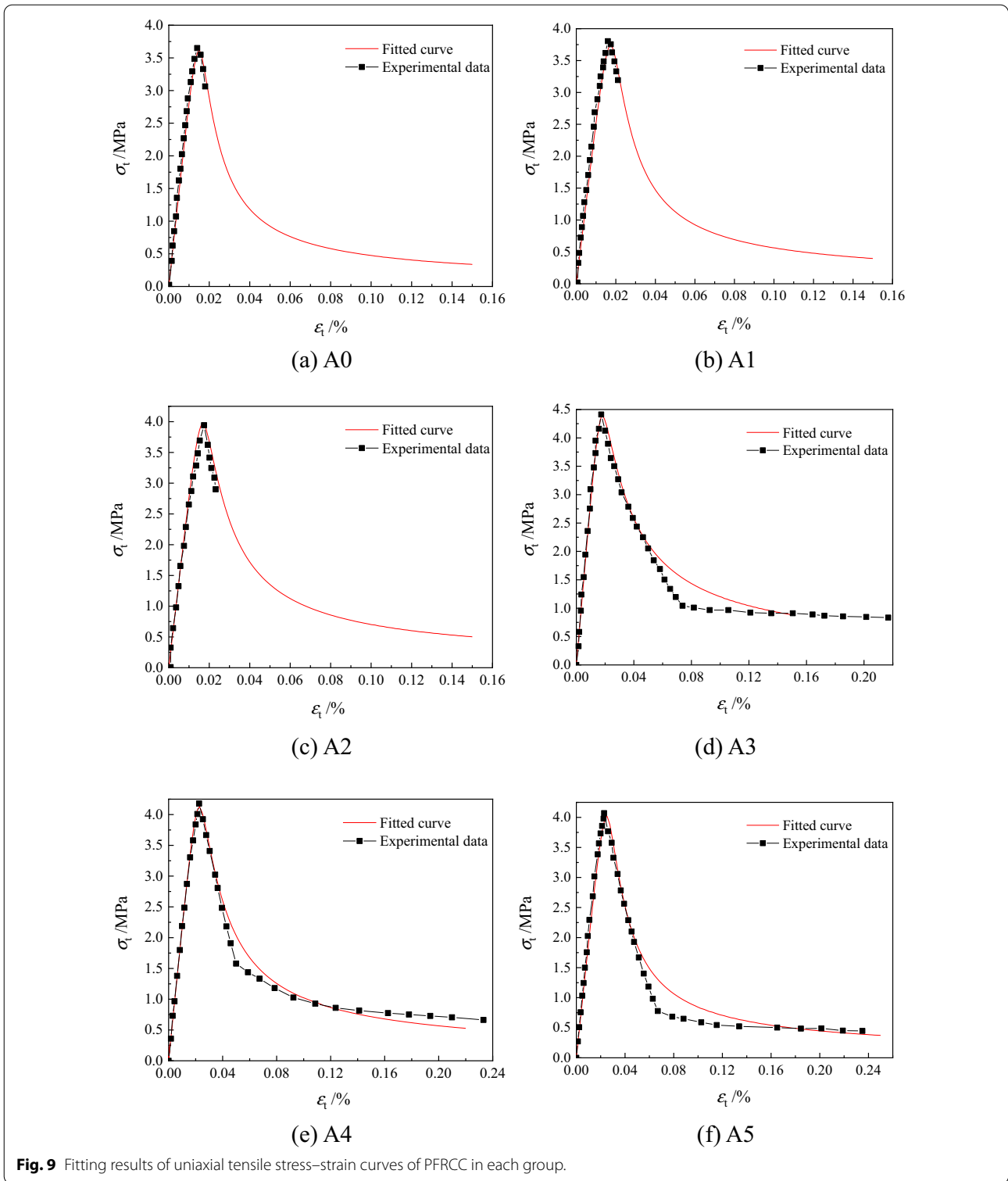


Fig. 9 Fitting results of uniaxial tensile stress–strain curves of PFRCC in each group.

3.4 PPF Enhancement Mechanism Analysis

The interfacial transition zone (ITZ) between aggregates and matrix is the decisive factor of the mechanical properties of concrete according to existing studies (Akçaoğlu

et al., 2005). It is the weak stress zone of concrete and easy to produce original cracks and defects. The deterioration of concrete under external load often appears firstly in ITZ, mainly attributed to that: ① the expansion

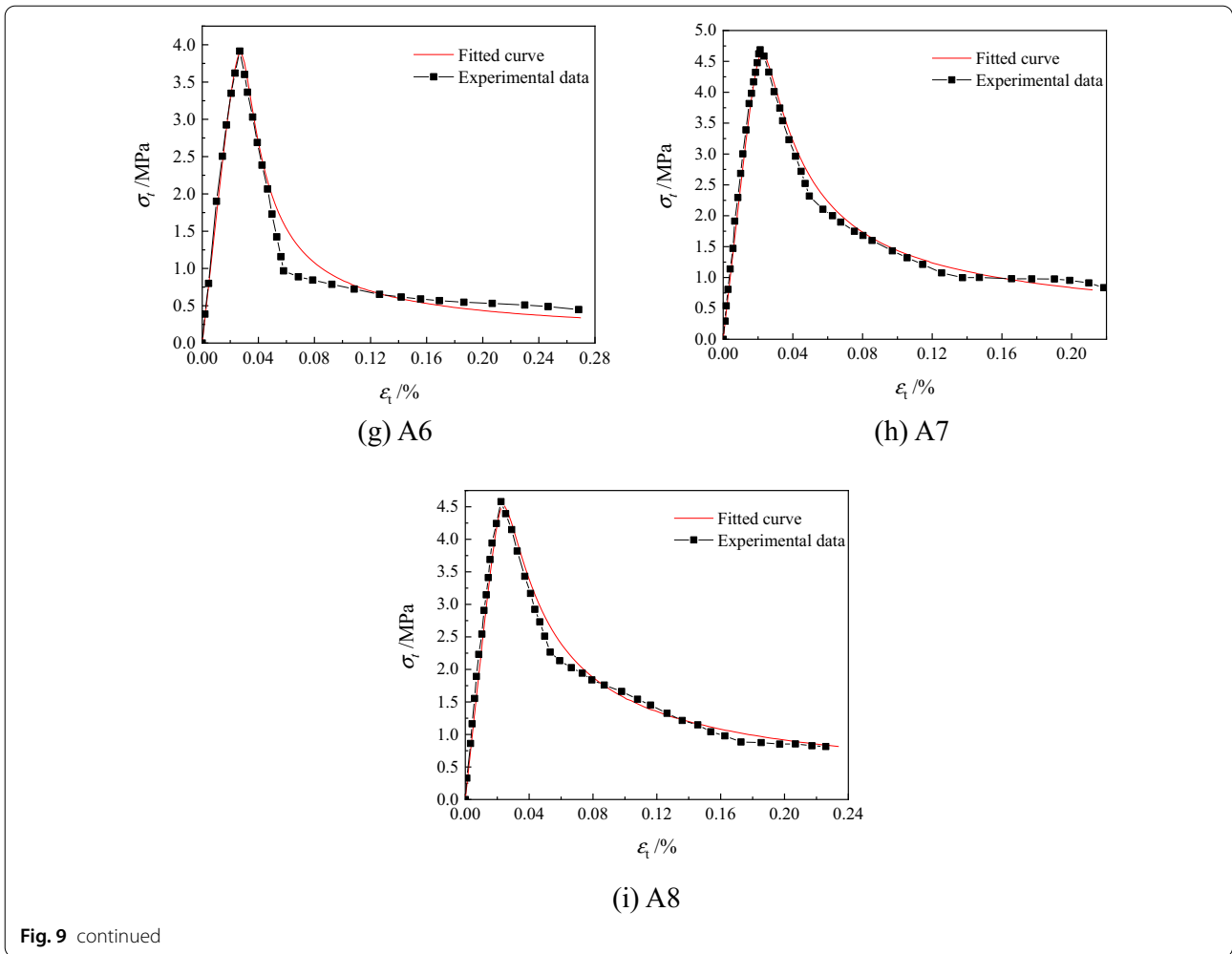


Table 8 The fiber volume fraction and characteristic value.

| Specimen no. | $V_{FF1}/\%$ | $V_{FF2}/\%$ | $V_{CF}/\%$ | λ_i | λ_j | λ_k |
|--------------|--------------|--------------|-------------|-------------|-------------|-------------|
| A0 | 0 | 0 | 0 | 0 | 0 | 0 |
| A1 | 0.099 | 0 | 0 | 0.72 | 0 | 0 |
| A2 | 0 | 0.099 | 0 | 0 | 0.188 | 0 |
| A3 | 0 | 0 | 0.632 | 0 | 0 | 0.395 |
| A4 | 0.066 | 0 | 0.568 | 0.48 | 0 | 0.355 |
| A5 | 0.099 | 0 | 0.537 | 0.72 | 0 | 0.336 |
| A6 | 0.132 | 0 | 0.505 | 0.96 | 0 | 0.316 |
| A7 | 0.049 | 0.049 | 0.537 | 0.36 | 0.094 | 0.336 |
| A8 | 0.066 | 0.066 | 0.505 | 0.480 | 0.125 | 0.316 |

coefficient of the aggregates and cement matrix is greatly different. ② in the stress hardening process of concrete, the water in the cement paste migrates to the hydrophilic aggregate surface, making the aggregate surface to form a layer of water film and leaving fine pores in concrete.

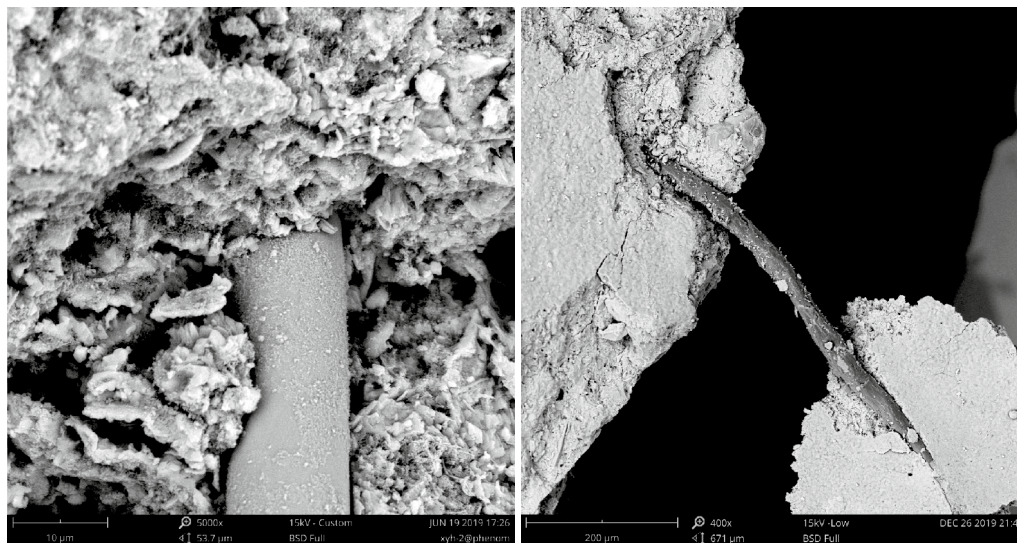
Therefore, when the concrete is affected by external forces, with the increase of internal stress, these existing microcracks are constantly connected and expanded, which eventually caused the damage of concrete.

Table 9 The enhancement coefficient W by fitting the fiber hybrid effect function.

| Mechanical indexes | The enhancement coefficient W of PFRCC | R^2 |
|--------------------|--|-------|
| f_t | $W_{f_t} = 1 + 0.0907 \times \lambda_i + 1.0588 \times \lambda_j + 1.0618 \times \lambda_k - 0.063 \times \lambda_j^2 - 2.816 \times \lambda_j^2 - 1.344 \times \lambda_k^2 - 0.824 \times \lambda_i \lambda_j + 4.064 \times \lambda_j \lambda_k - 0.520 \times \lambda_k \lambda_i - 5.243 \times \lambda_i \lambda_j \lambda_k$ | 0.999 |
| ε_t | $W_{\varepsilon_t} = 1 + 0.3744 \times \lambda_i + 1.2946 \times \lambda_j + 0.8485 \times \lambda_k - 0.260 \times \lambda_j^2 - 3.443 \times \lambda_j^2 - 1.074 \times \lambda_k^2 + 1.741 \times \lambda_i \lambda_j - 4.064 \times \lambda_j \lambda_k + 1.637 \times \lambda_k \lambda_i - 0.075 \times \lambda_i \lambda_j \lambda_k$ | 0.988 |
| α_t | $W_{\alpha_t} = 1 - 0.0605 \times \lambda_i - 2.2195 \times \lambda_j - 2.7421 \times \lambda_k + 0.042 \times \lambda_j^2 + 5.903 \times \lambda_j^2 + 3.471 \times \lambda_k^2 - 1.678 \times \lambda_i \lambda_j + 4.353 \times \lambda_j \lambda_k + 2.089 \times \lambda_k \lambda_i - 10.035 \times \lambda_i \lambda_j \lambda_k$ | 0.798 |
| E_c | $W_{E_c} = 1 + 0.0547 \times \lambda_i + 0.4674 \times \lambda_j + 0.1311 \times \lambda_k - 0.038 \times \lambda_j^2 - 1.243 \times \lambda_j^2 - 0.166 \times \lambda_k^2 + 0.827 \times \lambda_i \lambda_j + 2.621 \times \lambda_j \lambda_k - 0.154 \times \lambda_k \lambda_i - 12.991 \times \lambda_i \lambda_j \lambda_k$ | 0.979 |

Fig. 5 indicates that the incorporation of PPF can increase the compressive strength of RCC, and the hybridization of micro- and macro-PPF showed a significantly synergistic effect. In the process of mixing, the uniform dispersion of thousands of fibers in concrete can play the role of supporting aggregate and limiting aggregate sinking, reducing concrete bleeding and plastic shrinkage cracking. The PPFs are tightly bonded to the concrete matrix, as shown in Fig. 10(a).

The micro-PPFs play a major role in separating and connecting the pores, so that the pores in the concrete can be refined. Moreover, the incorporation of macro-PPF can obviously improve the brittle failure of concrete. The corrugated and relatively large surface area of macro-PPF can enhance the stiffness of PPF and the mechanical bite force between the PPF and concrete matrix, improving the bridging effect at the cracks. Fig. 5 shows that the compressive strength of multi-scale PFRCC all



(a) Bonding between PPF and concrete matrix

(b) Bridging effect of PPF

Fig. 10 The SEM image of fibers in concrete matrix.

performed well at different curing ages. PPFs of three different sizes, shapes and mechanical properties play a role in different cracking levels of RCC, so that they will be complementary by each other to produce a composite effect. When the macro- and micro-PPFs are mixed, they are tightly wrapped by hydrates and bonded to each other to form the network reinforcement system, alleviating the stress concentration at the top of crack and improving the densification and integrity of RCC structure, thus increasing the compressive strength of RCC (Hsie et al., 2008).

The tensile damage of fiber-reinforced concrete usually results from the expansion of transverse cracks and the decrease of the effective stress area. The distribution of PPFs in concrete is presented in Fig. 11 (Pakravan et al., 2017). As depicted in Fig. 11, the micro-PPF can bridge the microcracks in concrete matrix and control the coalescence of microcracks, enhancing the early tensile performance of RCC. Moreover, the macro-PPF across the macrocracks can play a bridging role in bounding the relative displacement of the matrix around the microcrack and reduce the stress concentration on the top of the microcrack (Yin et al., 2015), as shown in Fig. 10(b) and Fig. 11. Macro-PPF mainly bridges the RCC matrix after tensile failure and supports the tensile load lower than its tensile strength or cement bond strength. The PPFs that are not parallel to the fracture surface can dissipate the stress field nearby the top of crack and limit the crack expansion. When the total PPF content is constant, the stress concentration at the crack top is gradually reduced due to the decrease of the fiber spacing and the enhancement of the interaction between PPF and RCC. PPFs of different scales play a different role in different cracking stages of RCC. The crack resistance effect of micro-PPF and macro-PPF has its own characteristics and cannot be replaced by each other. The performance of

RCC will improve greatly by mixing PPFs of different scales in concrete matrix in a certain amount and proportion. The network structure formed by macro-PPF and micro-PPF randomly distributed in RCC lower the stress concentration at the cracks tip and more microcracks are needed to absorb energy in RCC, which explains the reason for the increase in the tensile strength and toughness of hybrid PFRCC specimens as shown in Figs. 6 and 8.

4 Conclusions

Through the above research on the effect of hybrid effect of polypropylene fibers on the compressive strength, splitting tensile strength and axial tensile properties of RCC, the main conclusions can be summarized as follows:

- (1) The addition of micro-PPF had a significant effect on the compressive and splitting tensile strength of RCC within 7 days, and the addition of macro-PPF played a major role in RCC after curing for 7 days. The compressive and splitting tensile strength of multi-scale PFRCC specimens A7 and A8 were the highest in all groups, showing a positive fiber hybrid effect of PPFs of three types.
- (2) With the addition of PPF, the uniaxial tensile strength f_t , the tensile strain ε_t , the tensile energy $W_{0.2}$ and the uniaxial tensile toughness ratio $R_{e,0.2}$ of RCC specimens were increased by 4~28%, 12~83%, 21~767%, and 15~585%, respectively.
- (3) The uniaxial tensile constitutive equation of concrete proposed in Chinese standard GB 50010-2010 can better adapt to PFRCC and the correction determination coefficient R^2 were greater than 0.97 for all testing groups. The proposed fiber hybrid effect function was also in good agreement with the experimental results, providing reference for theoretical research and engineering application.
- (4) The single PPF can promote the mechanical properties of RCC, but PPFs of different types showed obvious positive hybrid effect. The crack resistance effect of micro-PPF and macro-PPF cannot be replaced by each other. The performance of RCC can be improved with the incorporation of PPF of different sizes in a reasonable proportion.

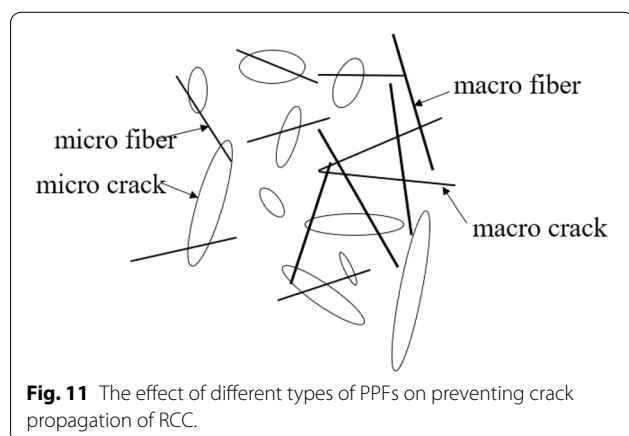


Fig. 11 The effect of different types of PPFs on preventing crack propagation of RCC.

Acknowledgements

This study is supported by horizontal research (H20211094), graduate scientific research and innovation foundation of Chongqing, China (Grant No. CYS20023 and CYS20027) and Chongqing Basic and Frontier Research Project (cstc2018jscx-mszdX0071). The authors gratefully acknowledge these supports.

Authors' contributions

LNH: conceptualization, validation, formal analysis, investigation, writing final draft, writing—review/editing, visualization. YXF: data curation, original draft, writing—review/editing, formal analysis, and data curation. YR: experimentation, writing—review/editing. MQX: experimentation, writing—review/editing. LXR: supervision and project administration. All authors read and approved the final manuscript.

Authors' information

Ninghui Liang, Associate Professor, Department of Civil Engineering and National Joint Engineering Research Center for Prevention and Control of Environmental Geological Hazards in the TGR area, College of Civil Engineering, Chongqing University, Chongqing 400,045, China. Email: liangninghui0705@163.com.

Xiufei You, Graduate Student, Department of Civil Engineering and National Joint Engineering Research Center for Prevention and Control of Environmental Geological Hazards in the TGR area, College of Civil Engineering, Chongqing University, Chongqing 400,045, China. Email: yxf_0723@163.com.

Ru Yan, Structural Engineer, Powerchina Chengdu Engineering Co.,Ltd, Chengdu Sichuan, China. Email: 1,271,735,867@qq.com.

Qingxu Miao, Verification Service Engineer, China Merchants Chongqing Highway Engineering Testing Center Co., Ltd, Chongqing, China. Email: miaoqingxu_123@163.com.

Xinrong Liu, Professor, Department of Civil Engineering and National Joint Engineering Research Center for Prevention and Control of Environmental Geological Hazards in the TGR area, College of Civil Engineering, Chongqing University, Chongqing 400,045, China. Email: liuxinrong@126.com

Funding

Graduate scientific research and innovation foundation of Chongqing, China (Grant No. CYS20027) and Chongqing Basic and Frontier Research Project (cstc2018jcsx-mszdX0071).

Availability of data and materials

The data and materials are included in the manuscript.

Declarations

Competing interests

The authors declare no competing financial interest regarding this publication.

Author details

¹School of Civil Engineering, Chongqing University, Chongqing, China.

²Powerchina Chengdu Engineering Co., Ltd, Chengdu Sichuan, China. ³China Merchants Chongqing Highway Engineering Testing Center Co., Ltd, Chongqing, China.

Received: 7 September 2021 Accepted: 9 December 2021

Published online: 11 January 2022

References

- Aghaeipour, A., & Madhkan, M. (2019). Mechanical properties and durability of roller compacted concrete pavement (RCCP)—a review. *Road Materials and Pavement Design*, 21(7), 1775–1798.
- Ahmad, S., & Umar, A. (2018). Rheological and mechanical properties of self-compacting concrete with glass and polyvinyl alcohol fibres. *Journal of Building Engineering*, 17, 65–74.
- Akçaoğlu, T., Tokyay, M., & Çelik, T. (2005). Assessing the ITZ microcracking via scanning electron microscope and its effect on the failure behavior of concrete. *Cement and Concrete Research*, 35(2), 358–363.
- Bayagoob, K. H., & Bamaga, S. O. (2019). Construction of roller compacted concrete dams in hot arid regions. *Materials (basel)*, 12(19), 3064.
- Benouadah, A., Beddar, M., & Meddah, A. (2017). Physical and mechanical behaviour of a roller compacted concrete reinforced with polypropylene fiber. *Journal of Fundamental and Applied Sciences*, 9(2), 623.
- Cattaneo, S., Rosati, G., & Banthia, N. (2009). A simple model to explain the effect of different boundary conditions in direct tensile tests. *Construction and Building Materials*, 23(1), 129–137.
- CECS 13:2009. "Standard test methods for fiber reinforced concrete." National Standard of the People's Republic of China. (in Chinese)
- DL/T5330-2015. Code for mix design of hydraulic concrete. National Standard of the People's Republic of China. (in Chinese)
- Deng, Z. Y., Liu, X. R., Yang, X., et al. (2020). A study of tensile and compressive properties of hybrid basalt-polypropylene fiber-reinforced concrete under uniaxial loads. *Structural Concrete*. <https://doi.org/10.1002/suco.202000006>
- Ding, Y. N., & Yan, Y. C. (2011). Experimental investigation on uniaxial tensile properties of steel fiber reinforced concrete. *Applied Mechanics and Materials*, 94–96, 731–735.
- GB/T 17671-1999. Methods of testing cements—Determination of strength. National Standard of the People's Republic of China.(in Chinese)
- GB 8076-2008. "Concrete admixtures" National Standard of the People's Republic of China. (in Chinese).
- GB 50010-2010. Code for design of concrete structures. National Standard of the People's Republic of China. (in Chinese)
- GB/T 1346-2011. Test methods for water requirement of normal consistency, setting time and soundness of the Portland cement. National Standard of the People's Republic of China. (in Chinese)
- GB/T 50080-2016. "Standard for test method of performance on ordinary fresh concrete. National Standard of the People's Republic of China. (in Chinese)
- GB/T50081-2019. "Standard for test methods of concrete physical and mechanical properties." National Standard of the People's Republic of China. (in Chinese)
- Guo, Z. H., & Shi, X. D. (2003). *Reinforced concrete theory and analyse*. Beijing: Tsinghua University Press. (in Chinese).
- Hsie, M., Tu, C., & Song, P. S. (2008). Mechanical properties of polypropylene hybrid fiber-reinforced concrete. *Materials Science and Engineering: A*, 494(1–2), 153–157.
- Hu, A., Liang, X., Yu, J., et al. (2018). Tensile characteristics of ultra-high-performance concrete. *Magazine of Concrete Research*, 70(6), 314–324.
- Hussain, I., Ali, B., Akhtar, T., et al. (2020). Comparison of mechanical properties of concrete and design thickness of pavement with different types of fiber-reinforcements (steel, glass, and polypropylene). *Case Studies in Construction Materials*, 13, e00429.
- JGJ 52-2006. "Standard for technical requirements and test method of sand and crushed stone (or gravel) for ordinary concrete." National Standard of the People's Republic of China. (in Chinese)
- JGJ55-2011. "Specification for mix proportion design of ordinary concrete." National Standard of the People's Republic of China. (in Chinese)
- LaHucik, J., Dahal, S., Roesler, J., et al. (2017). Mechanical properties of roller-compacted concrete with macro-fibers. *Construction and Building Materials*, 135, 440–446.
- Lam, M. N. T., Le, D. H., & Jaritngam, S. (2018). Compressive strength and durability properties of roller-compacted concrete pavement containing electric arc furnace slag aggregate and fly ash. *Construction and Building Materials*, 191, 912–922.
- Liang, N. H., Dai, J. F., & Liu, X. R. (2016). Study on tensile damage constitutive model for multiscale polypropylene fiber concrete. *Advances in Materials Science and Engineering*, 2016, 1–6.
- Liang, N. H., Yan, R., Miao, Q. X., et al. (2021). Effect of multi-scale polypropylene fiber hybridization on compressive constitutive mechanics parameters of roller compacted concrete. *Structural Concrete*. <https://doi.org/10.1002/suco.202000117>
- Lisantino, A., Praja, B.A., & Hermawan, B.N. (2017) Flexural strength of self-compacting fiber reinforced concrete beams using polypropylene fiber: An experimental study. American Institute of Physics Conference Series.
- Liu, X. R., Yang, X., & Liang, N. H. (2015). A damage constitutive model for multi-scale polypropylene fiber concrete under compression and its numerical implementation. *Journal of Reinforced Plastics and Composites*, 34(17), 1403–1412.
- Lopez-Uceda, A., Agrela, F., Cabrera, M., et al. (2016). Mechanical performance of roller compacted concrete with recycled concrete aggregates. *Road Materials and Pavement Design*, 19(1), 36–55.
- Madhkan, M., Azizkhani, R., & Torki, M. E. (2011). Roller compacted concrete pavements reinforced with steel and polypropylene fibers. *Structural Engineering and Mechanics*, 40(2), 149–165.

- Madhkhani, M., Azizkhani, R., & Torki, M. E. (2012). Effects of pozzolans together with steel and polypropylene fibers on mechanical properties of RCC pavements. *Construction and Building Materials*, 26(1), 102–112.
- Marushchak, U. D., Sydor, N. I., & Soltysik, R. A. (2019). Modified fiber reinforced concrete for industrial floors. In IOP Conference series: Materials science and engineering, vol. 798(1).
- Olivito, R. S., & Zuccarello, F. A. (2010). An experimental study on the tensile strength of steel fiber reinforced concrete. *Composites Part b: Engineering*, 41(3), 246–255.
- Pakravan, H. R., Latifi, M., & Jamshidi, M. (2017). Hybrid short fiber reinforcement system in concrete: A review. *Construction and Building Materials*, 142, 280–294.
- Pyo, S., Kim, H. K., & Lee, B. Y. (2017). Effects of coarser fine aggregate on tensile properties of ultra high performance concrete. *Cement and Concrete Composites*, 84, 28–35.
- Rooholamini, H., Hassani, A., & Aliha, M. R. M. (2018). Fracture properties of hybrid fibre-reinforced roller-compacted concrete in mode I with consideration of possible kinked crack. *Construction and Building Materials*, 187, 248–256.
- Shao, X. R. (2011). Experiments for strength properties of polypropylene fiber-reinforced concrete. *Advanced Materials Research*, 194–196, 1030–1034.
- Simões, T., Octávio, C., Valença, J., et al. (2017). Influence of concrete strength and steel fibre geometry on the fibre/matrix interface. *Composites Part b: Engineering*, 122, 156–164.
- Turk, K., Bassurucu, M., & Bitkin, R. E. (2021). Workability, strength and flexural toughness properties of hybrid steel fiber reinforced SCC with high-volume fiber. *Construction and Building Materials*, 266, 120944.
- Xu, L. H., Mei, G. D., Huang, L., et al. (2014). Study on uniaxial tensile stress-strain relationship of steel-polypropylene hybrid fiber reinforced concrete. *China Civil Engineering Journal*, 47(07), 35–45. (in Chinese).
- Yao, W., Li, J., & Wu, K. (2003). Mechanical properties of hybrid fiber-reinforced concrete at low fiber volume fraction. *Cement and Concrete Research*, 33(1), 27–30.
- Yazici, Ş., Mardani-Aghabaglou, A., Tuyan, M., et al. (2015). Mechanical properties and impact resistance of roller-compacted concrete containing polypropylene fibre. *Magazine of Concrete Research*, 67(16), 867–875.
- Yin, S., Tuladhar, R., Shi, F., et al. (2015). Use of macro plastic fibres in concrete: A review. *Construction and Building Materials*, 93, 180–188.
- Yoo, D. Y., & Banthia, N. (2016). Mechanical properties of ultra-high-performance fiber-reinforced concrete: A review. *Cement and Concrete Composites*, 73, 267–280.
- Yuan, T. F., Lee, J. Y., & Yoon, Y. S. (2020). Enhancing the tensile capacity of no-slump high-strength high-ductility concrete. *Cement and Concrete Composites*, 106, 103458.

Publisher's Note

Springer Nature remains neutral with regard to jurisdictional claims in published maps and institutional affiliations.

Submit your manuscript to a SpringerOpen[®] journal and benefit from:

- Convenient online submission
- Rigorous peer review
- Open access: articles freely available online
- High visibility within the field
- Retaining the copyright to your article

Submit your next manuscript at ► [springeropen.com](https://www.springeropen.com)
